Nucleon Momentum Distributions in Asymmetric Nuclei

A Comparison of ${}^{3}\mathrm{He}(e, e'p)$ and ${}^{3}\mathrm{H}(e, e'p)$

A proposal to Jefferson Lab PAC 40, June 2013

C. Hyde, S.E. Kuhn and L.B. Weinstein (co-spokesperson)
Old Dominion University, Norfolk VA

M. Braverman, O. Hen (co-spokesperson), I.
Korover, J. Lichtenstadt, E. Piasetzky, and I. Yaron
Tel-Aviv University, Tel Aviv, Israel

W. Boeglin (co-spokesperson), P. Markowitz and M. Sargsian
Florida International University, Miami, FL

W. Bertozzi, S. Gilad (co-spokesperson), and V. Sulkosky
Massachusetts Institute of Technology, Cambridge, MA

Guy Ron
Hebrew University, Jerusalem, Israel

R. Gilman
Rutgers University, New Brunswick, NJ

J.W. Watson
Kent State University, Kent, OH

A. Beck and S. Maytal-Beck
Nuclear Research Center Negev, Beer-Sheva, Israel

D.W. Higinbotham, C. Keppel, P. Solvignon and S.A. Wood
Thomas Jefferson National Accelerator Facility, Newport News, VA

J. Beričič, M. Mihovilovič, S. Širca, and S. Štajner
Jožef Stefan Institute, Ljubljana, Slovenia

D. Keller
University of Virginia, Charlottesville, VA

L. Kaptari
Bogoliubov Lab. Theor. Phys., 141980, JINR, Dubna, Russia

(Dated: May 6, 2013)

We propose to take advantage of the installation of a ^{3}H target in Hall A and to make the first measurement of the quasielastic ^{3}H$(e, e'p)nn$ reaction using the MARATHON target and the two HRS spectrometers. We will compare this to the $d(e, e'p)n$, ^{3}He$(e, e'p)np$ and ^{3}He$(e, e'p)d$ reactions in order to learn about the ground state momentum distribution of protons in ^{3}H compared to ^{3}He. We will perform these measurements in kinematics where theoretical calculations and $d(e, e'p)$ measurements have shown Final State Interactions (FSI) to be small. In addition, the residual effects of FSI should be similar in ^{3}He and ^{3}H and therefore largely cancel in the ratio.

In the simplest picture, we expect the ratio of ^{3}He$(e, e'p)$ to ^{3}H$(e, e'p)$ to be two at low missing momentum due to simple proton counting. This ratio should decrease to one at larger missing momentum ($300 \leq p_{miss} \leq 500$ MeV/c) due the dominance of short range correlated np pairs (and the fact that there are two np pairs in each of ^{3}He and ^{3}H). We want to confirm these values and to map out the transition region where the ratio changes from two to one.

On a more quantitative level, we will take advantage of the fact that these few-nucleon systems are exactly calculable to use these measurements to reliably extract the nucleon ground-state high momentum distributions in these systems.
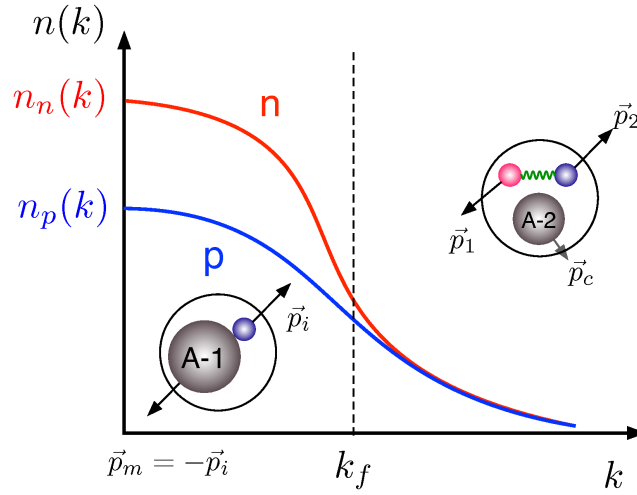
I. INTRODUCTION AND MOTIVATION

A. Nucleon Momentum Distributions in Heavy Asymmetric Nuclei

Recent double and triple coincidence experiments on carbon show that high momentum protons are predominantly paired with high momentum neutrons in np short range correlations (SRC) [1–3]. High momentum in this case means that the nucleon momentum is above the typical nuclear Fermi momentum of $k_F \approx 250$ MeV/c. This np dominance of these SRC is explained by the dominance of the tensor part of the nucleon-nucleon interaction [4–6].

In heavy asymmetric nuclei ($N > Z$) there are more neutrons than protons. However, due to the dominance of np-SRC pairs, there are approximately equal numbers of protons and neutrons with momenta $p \geq k_F$. That means that in these asymmetric nuclei the protons must move faster (have higher average momentum and kinetic energy) than neutrons (see Fig. 1) [7].
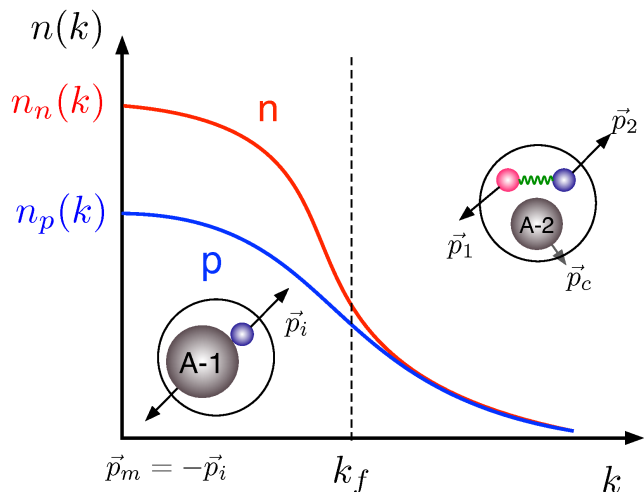

FIG. 1: Illustration of the momentum distribution of protons and neutrons in asymmetric nuclei. $n_n(k)$ and $n_p(k)$ are the neutron and proton momentum densities, respectively. The insets show the single nucleon in a mean field and the 2N-SRC pairs that dominate below and above k_F, respectively.

Recently a linear correlation between the EMC effect and the number of SRC pairs was demonstrated [8, 9]. Related to this, there is also a clear linear correlation between the EMC effect and the average nucleon separation energy [10] (see Fig. 2). The two observations are connected since high momentum nucleons belong to SRC pairs and have a larger separation energy. These observations can naturally be explained if the EMC effect is associated with large momentum (large virtuality) nucleons in nuclei.

The difference between the momentum distribution of protons and neutrons in asymmetric nuclei ($y = (N - Z)/(N + Z) = 0.2$ for Pb) might have major implications for nuclear physics and related fields. In asymmetric nuclei, the difference between the average kinetic
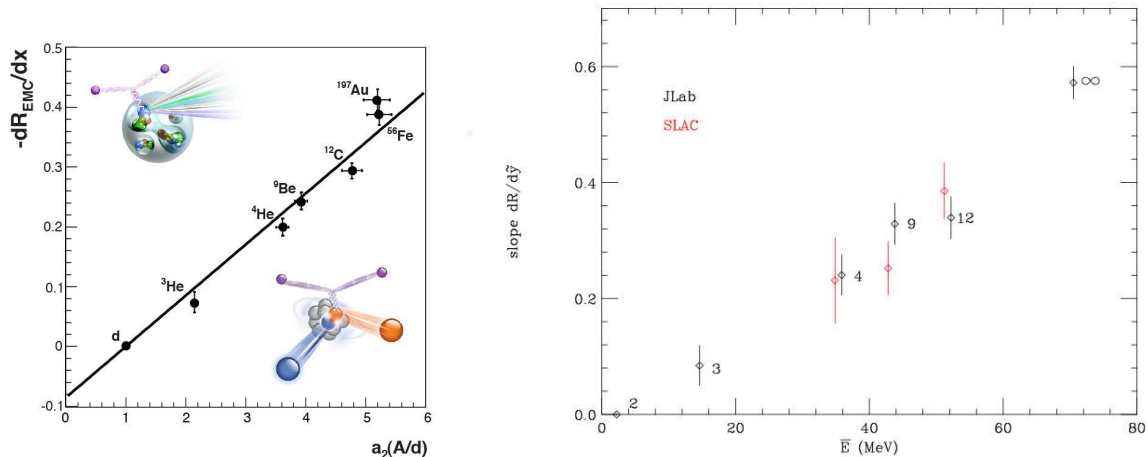
FIG. 2: Left: Linear correlation between the strength of the EMC effect and the amount of 2N-SRC in nuclei [9]. Right: Linear correlation between the strength of the EMC effect and the average nucleon separation energy [10].

energy per proton and per neutron leads to an isospin-dependent Deep-Inelastic scattering EMC effect and might be a natural explanation for the neutrino scattering NuTeV effect [11]. In addition, the effect of the asymmetric energy term on the neutron star equation of state and hence on neutrino cooling might be very significant [12].

B. Nucleon momentum distributions in light asymmetric nuclei

The results and interpretations discussed above can be confirmed in a unique way by studying proton and neutron momentum distributions in ^{3}He and ^{3}H nuclei. Reliable microscopic calculations are available for both of these nuclei. Their asymmetries are larger than those of any heavy asymmetric nucleus:

$$y_{A=3} = \frac{N-Z}{N+Z} = \pm 0.3 \quad .$$

The high momentum part of the nuclear momentum distribution should be dominated by the momentum distribution of the nucleons in correlated pairs. ^{3}He and ^{3}H both can form two np-pairs. We therefore expect that in ^{3}He the average kinetic energy of the neutron will be greater than that of each proton and vice versa in ^{3}H.

We know from prior experiments that $\sim$10% of nucleons in ^{3}He are in NN-SRC pairs [13], that np pairs are far more probable than nn or pp pairs [1, 14], and that the nucleon momentum distribution is dominated by SRC pairs for momenta greater than some threshold

(referred as p_1) [15]. Thus, we expect to find more protons than neutrons in ^{3}He at low nucleon momentum but equal numbers of protons and neutrons at high momentum (see Fig. 1). This picture will be reversed for ^{3}H, where we expect to find more neutrons than protons at low momentum but equal numbers of neutrons and protons at high momentum.

Below p_1, where independent nucleons dominate, the ratio of the proton momentum distribution to the neutron momentum distribution equals Z/N (i.e., two for ^{3}He and 0.5 for ^{3}H). In contrast, the ratio of proton to neutron momentum distributions above p_1, where 2N-SRC dominates, should be close to 1. In the regions where all three nucleons have high momentum, above some threshold momentum p_2, the ratio should revert back to Z/N. The expected ratios are shown in Fig. 3.
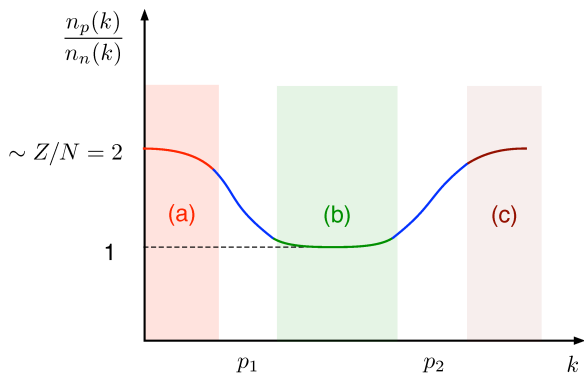

FIG. 3: The naively expected ratio of proton to neutron momentum densities as a function of initial momentum for ^{3}He. By isospin symmetry, this is also the expected ratio of the ^{3}He to ^{3}H proton momentum densities. The calculated ratio of these momentum densities is shown in Fig. 6.

There are no measurements of neutron momentum distributions in ^{3}He or of neutron or proton momentum distributions in ^{3}H. However, it is much easier experimentally to detect protons than neutrons. By isospin symmetry, we expect the proton momentum distribution in ^{3}H to equal the neutron momentum distribution in ^{3}He. The ratio of proton momentum distributions in ^{3}He and ^{3}H should therefore be the same as shown in Fig. 3.

We propose to measure this ratio with high accuracy by measuring the quasielastic knockout of protons from ^{3}He and ^{3}H. The interesting physics will come from (a) measuring these ratios for $p \ll p_1$ and for $p \gg p_1$ where we expect the ratios to be stable, (b) measuring the transition between these regions, and (c) observing deviations from this simple picture.

C. Calculated ground state momentum distributions for ^{3}He and ^{3}H

We propose to measure the $(e, e'p)$ cross section for ^{3}H rather than the $(e, e'n)$ cross section for ^{3}He. We expect the neutron momentum distribution in ^{3}He to be very similar to

the proton momentum distribution in ^{3}H. However, there are a lot of available calculations for ^{3}He and very few for ^{3}H. Therefore, we will show some calculations comparing the proton and neutron distributions in ^{3}He, rather than the proton distributions in ^{3}He and ^{3}H.

Fig. 4 shows the momentum distribution of the deuteron and of the proton and neutron in ^{3}He as well as the ratio of the p and n distributions in ^{3}He to that of the deuteron. The deuteron distributions are calculated using the Argonne V18 (AV18) NN potential [16–18]. The ^{3}He distributions are from Variational Monte Carlo calculations using the Argonne V18 + Urbana IX (AV18+UIX) Hamiltonian [16, 19]. The proton momentum distribution in ^{3}He is significantly greater than that of the neutron at low momenta but is approximately the same for $1.5 \leq k \leq 2.5$ fm^{-1} (corresponding to $300 \leq p \leq 500$ MeV/c). The deuteron momentum distribution and the neutron momentum distribution in ^{3}He for momenta $p \geq 150$ MeV/c are quite similar. Fig. 5 shows the same quantities calculated by Alvioli *et al.* [20].

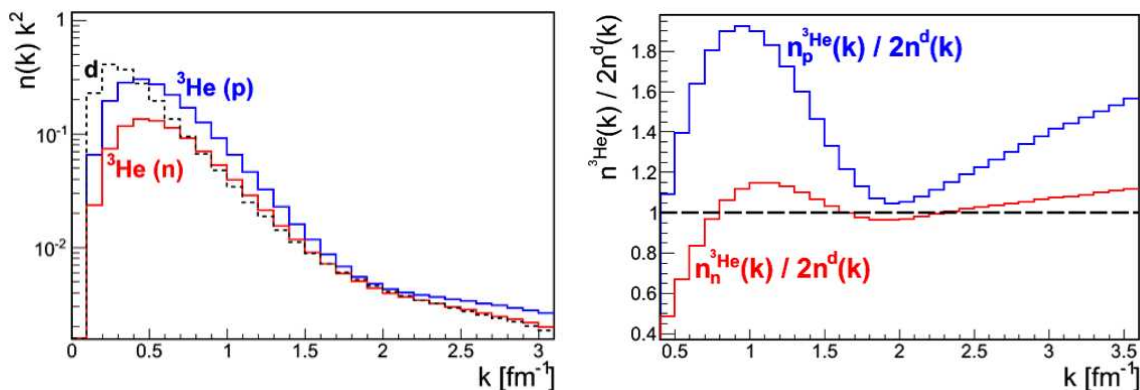

FIG. 4: (left) The momentum distributions of the proton and the neutron in ^{3}He and in deuterium [16–19]. (The proton's momentum distribution integral is normalized to $Z = 2$ and the neutron's to $N = 1$.) The deuterium distribution is multiplied by $a_2(^3\text{He}/d) = 2$, the ratio of the cross sections for ^{3}He(e, e') to $d(e, e')$ at $1.5 \leq x \leq 2$ [13]. (right) The ratio of the ^{3}He p and n momentum distributions to that of twice the deuteron.

2N-SRC dominate the momentum distribution starting at about $p = 275$ MeV/c [15]. The np-SRC dominance region is at about $300 \leq p \leq 500$ MeV/c where the momentum distributions of the n in ^{3}He, the p in ^{3}He, and the deuteron are similar. For $p \geq 500$ MeV/c, the proton momentum distribution in ^{3}He increases, showing the effect of configurations where all three nucleons have high momentum (e.g., 3N-SRC).

Similar calculations by Claudio Ciofi degli Atti and collaborators show the ratio of Plane Wave Impulse Approximation (PWIA) calculations of proton to neutron knockout from ^{3}He
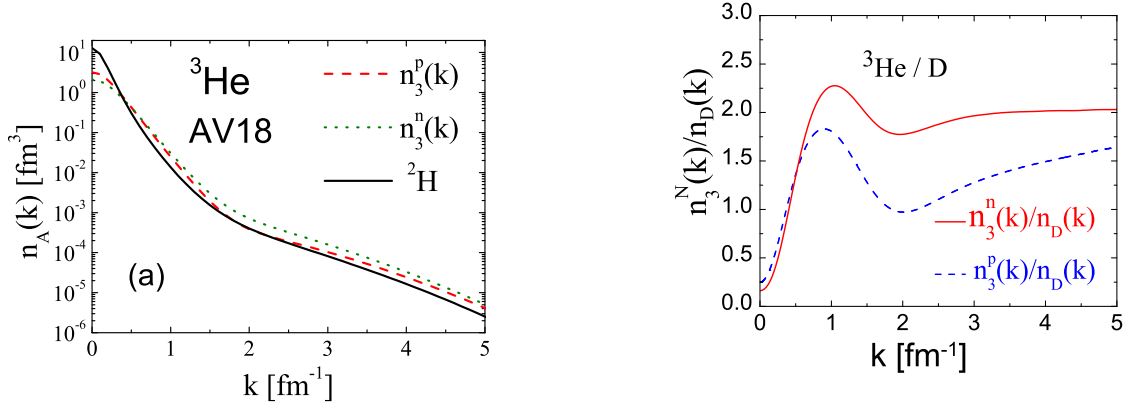
FIG. 5: (left) The momentum distributions of the proton and the neutron in ^{3}He and in deuterium. The integrals of the momentum distributions are normalized to one. (right) The ratio of the ^{3}He p and n momentum distributions to that of the deuteron [20].

(see Fig. 6). These calculations do not include rescattering of the struck nucleon, but they do include the continuum interaction between the two non-struck nucleons. The ratio is large at small nucleon momentum, decreases to 1 at $p_m = 400$ MeV/c and then increases again. This picture is qualitatively similar to the cartoon ratio shown in Fig. 3.
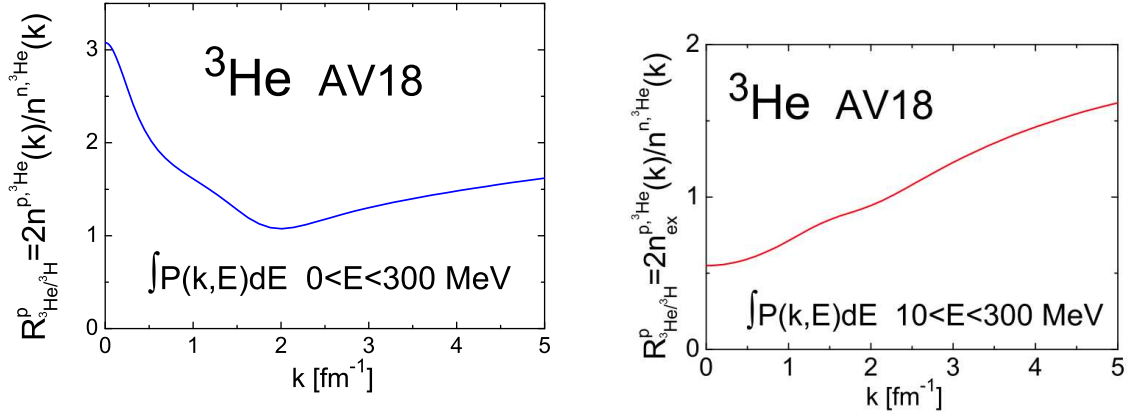

FIG. 6: The ratio of reduced cross sections (PWIA cross sections divided by the electron-nucleon elementary cross section) for ^{3}He$(e, e'p)$ to ^{3}He$(e, e'n)$ calculated by Ciofi degli Atti, Kaptari and collaborators [20, 21]. The left panel includes both the 2-body and 3-body breakup channels of ^{3}He$(e, e'p)$ and the right panel includes only the 3-body breakup channel.

The above ratio includes the two-body-breakup (2BBU) and three-body-breakup (3BBU) channels of ^{3}He$(e, e'p)$. If we only include the 3BBU channel, then the ratio looks very different (see Fig. 6(right)). This is because the 2BBU channel dominates at low missing

momentum but is much less important at high missing momentum.

Thus, the actual theoretical picture, whether it includes just the momentum distribution, or integrates over the spectral function, or involves the ratio of reduced PWIA cross sections, is remarkably similar (at least qualitatively) to the simplistic picture we presented in sections I.A and I.B.

D. Previous Measurements

The most direct way of studying nucleon momentum distributions in nuclei is to measure the quasi-elastic (QE) ^{3}He$(e, e'p)$ and ^{3}H$(e, e'p)$ reactions as a function of missing momentum, $\vec{p}_m = \vec{q} - \vec{p}_p$, where $\vec{p}_p$ is the momentum of the outgoing, observed proton and $\vec{q}$ is the momentum transfer. The missing momentum, $\vec{p}_m$ equals $\vec{p}_r$, the momentum of the $A - 1$ recoil. Within the Plane Wave Impulse Approximation (PWIA) where Final State Interactions (FSI) are neglected, $\vec{p}_{init} = -\vec{p}_m$ where $\vec{p}_{init}$ is the initial momentum of the target nucleon before the interaction.
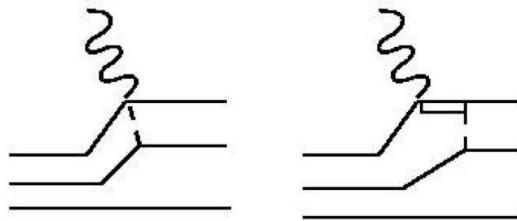

FIG. 7: Diagrams for Meson Exchange Currents (left) and Isobar Configurations (right).

However, depending on the selected kinematics, other reaction mechanisms can contribute to the cross section. The outgoing (struck) proton can rescatter from the other nucleons (FSI), or the virtual photon can couple to the exchanged meson (MEC) or or the virtual photon can excite the nucleon to an intermediate isobar state (IC). Fig. 7 shows schematically how IC and MEC can cause the measured missing momentum to be different from the genuine ground state (g.s) momentum distribution.

Due to these competing reaction channels, previous experiments at $Q^2 < 1$ (GeV/c)^2 [22–26] did not strongly constrain the high momentum components of the ground state

momentum distribution. The Jefferson Lab ^{3}He$(e, e'p)$ measurement was performed in perpendicular kinematics and the high-missing-momentum ($p_m \geq 300$ MeV/c) measurements were dominated by FSI (see Figs. 8 and 9) [26, 27]. The FSI domination is shown by the significant disagreement between PWIA calculations and the measured cross sections and by the relative agreement between calculations including FSI and those same cross sections. This FSI domination is not surprising, because small angle rescattering of the knocked-out proton contributes significantly at perpendicular kinematics.
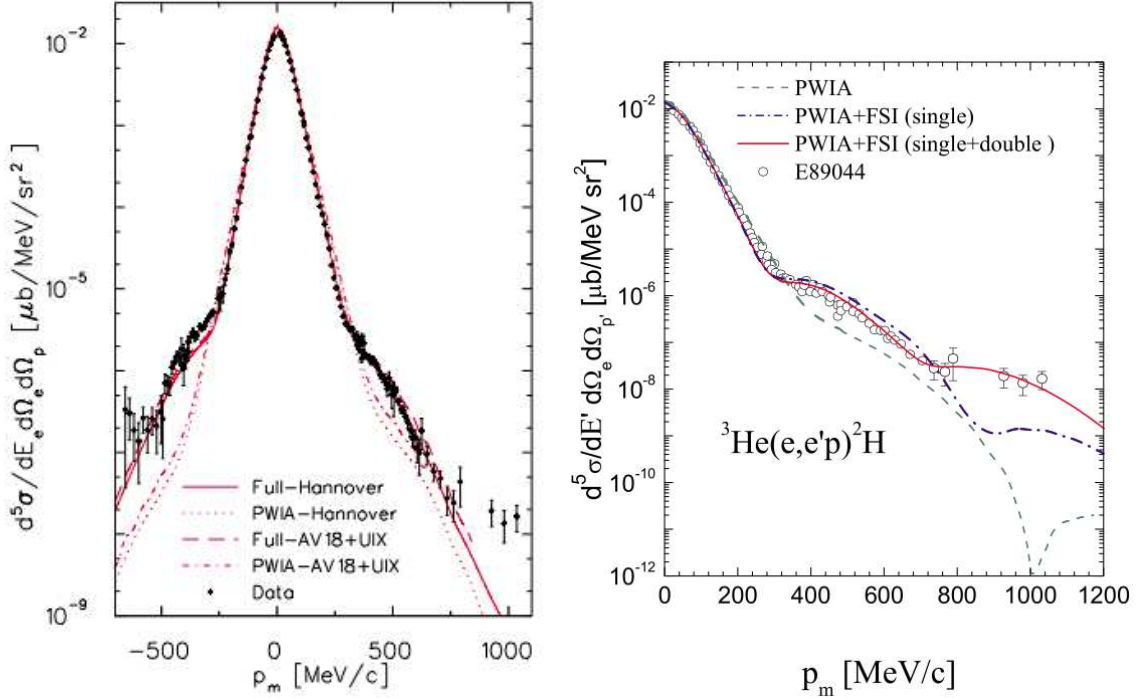

FIG. 8: The measured ^{3}He$(e, e'p)^2$H cross section as a function of the missing momentum p_m. The left figure also shows PWIA and full calculations in the diagrammatic approach by Laget for two different ground state wave functions (see [26] and references therein). The right figure shows the same data with calculations by Ciofi degli Atti and Kaptari [28]. The dashed line corresponds to the PWIA, the dot-dashed line includes FSI with single rescattering and the solid line includes both single and double rescattering [28].

E.   Minimizing Final State Interactions

Fortunately, measurements on the deuteron show that we can select kinematics to minimize the effects of FSI [32]. Fig. 10 shows that the impact of FSI on the cross section decreases rapidly as θ_{rq}, the angle between the recoil momentum ($\vec{p}_{recoil} = \vec{p}_m$) and $\vec{q}$, decreases from 75° to 35°.
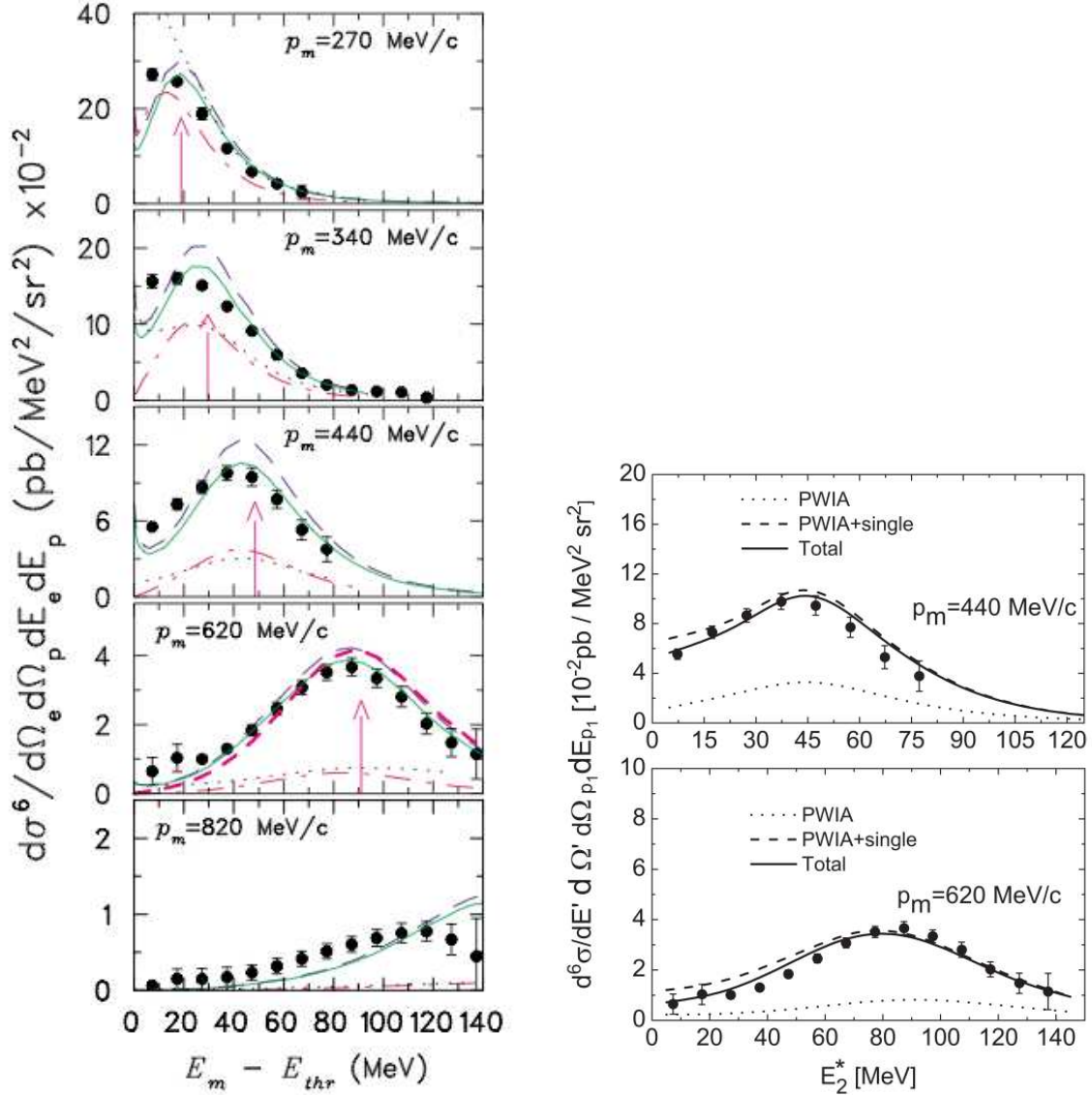
FIG. 9: (left) The cross section for the ^{3}He$(e, e'p)pn$ reaction as a function of missing energy [27]. The vertical arrow gives the peak position expected for disintegration of correlated pairs, $E_m = \omega - T_p - T_r = p_m^2/4m$ (where T_p is the kinetic energy of the detected proton and $T_r = p_m^2/2m_{A-1}$ is the kinetic energy of the recoiling $A-1$ "nucleus"). The black dotted curve presents a PWIA calculation using Salmes spectral function and σ_{cc1} electron-proton off-shell cross section and the red dash-dotted line is a Laget PWIA calculation. Other curves are Laget's calculations for PWIA+FSI (black long dashed line) and his full calculation (solid green line), including meson-exchange current and final-state interactions. In the 620 MeV/c panel, the additional bold red short dashed curve is a calculation with PWIA + FSI only within the correlated pair [29, 30]. (right) The same experimental cross section plotted vs $E_2^* = E_m - E_{thr}$ compared to the unfactorized calculations of Alvioli, Ciofi degli Atti and Kaptari [31]. The dotted line shows the PWIA calculation, the dashed line includes FSI with single rescattering and the solid line includes FSI with both single and double rescattering.
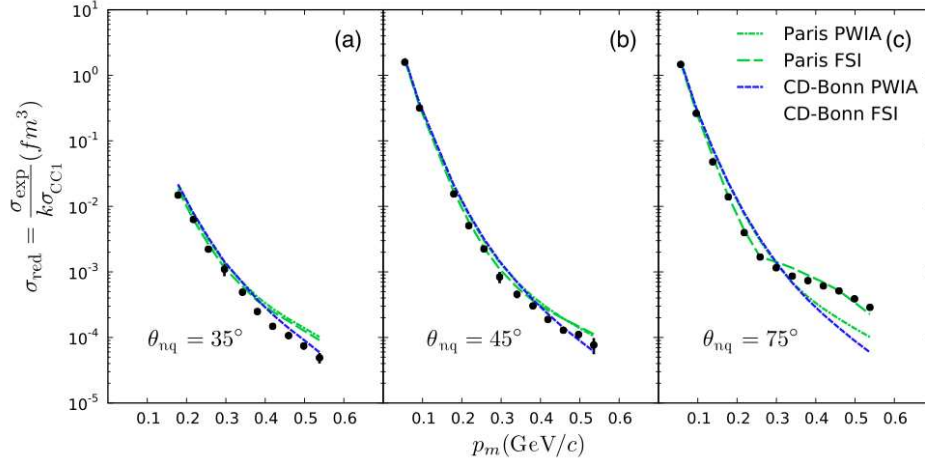
FIG. 10: The reduced cross section for $d(e, e'p)$ as a function of missing momentum for three different recoil angles, (a) $\theta_{rq} = 35°$, (b) $\theta_{rq} = 45°$, and (c) $\theta_{rq} = 75°$. All calculations are by M. Sargsian [32].

We expect the same FSI suppression to hold for the nucleons in the correlated pair in ^{3}He and ^{3}H. Calculations by Ciofi degli Atti [21] and by Sargsian [11] show that FSI are minimized at smaller values of θ_{rq}. Fig. 11 shows that the effects of FSI peak at $\theta_{rq} \approx 70°$ and are much smaller for $\theta_{rq} \leq 40°$.
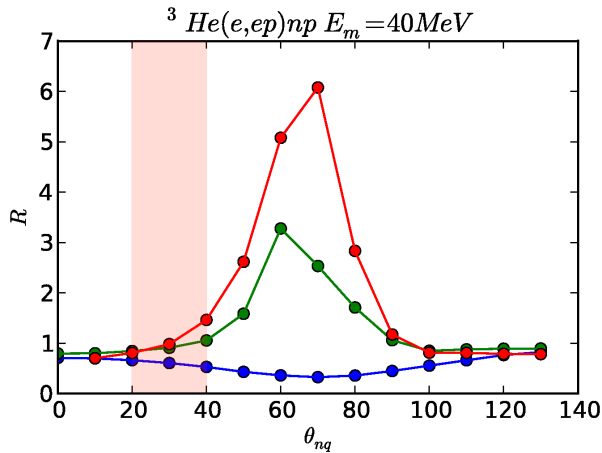

FIG. 11: The ratio of the FSI calculation which includes rescattering of the struck nucleon to the PWIA cross section for $p_m = 0.2$ (blue), 0.4 (green), and 0.5 (red) GeV/c as a function of θ_{rq}, the angle between the recoil momentum and $\vec{q}$ [11].

Fig. 12 shows the ratio of the FSI to PWIA calculations for a range of missing energies and missing momenta at a recoil angle $\theta_{rq} = 30°$. The ratios are almost all reasonably close to unity, especially for larger missing momenta.

We will significantly reduce the remaining effects of FSI by forming the ratio of ^{3}He$(e, e'p)$ to ^{3}H$(e, e'p)$. In the simplest picture, the struck proton has the same probability to rescatter from the other two nucleons whether it was knocked out of ^{3}He or ^{3}H.
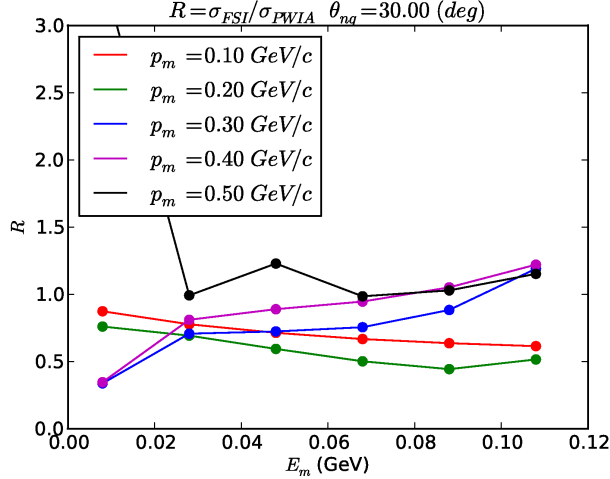
FIG. 12: The ratio of the FSI calculation which includes rescattering of the struck nucleon to the PWIA cross section as a function of missing energy $E_m = \omega - T_p - T_r$ for $\theta_{rq} = 30°$ and for various missing momenta [11].

In practice, calculations by Kaptari [33] show that in perpendicular kinematics at $p_m = 500$ MeV/c, where FSI increase the PWIA cross section by a factor of about four, they change the ratio of $^3\text{He}(e, e'p)$ to $^3\text{H}(e, e'p)$ by only 20–30% at the peak of the cross section (see Fig. 13). However, in perpendicular kinematics, the effects of FSI are additive because the rescattering shifts strength from smaller to larger missing momentum. Therefore, even though the PWIA and PWiA+FSI cross section ratios are similar, it is important to measure the cross section away from perpendicular kinematics to reduce the effect of FSI on both the cross sections and their ratios.
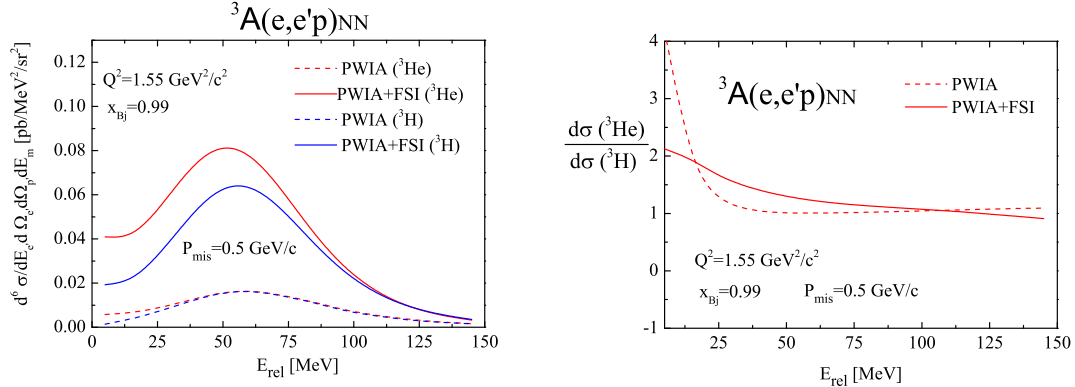

FIG. 13: (left) The $^3\text{He}(e, e'p)$ and $^3\text{H}(e, e'p)$ cross sections in perpendicular kinematics (kinematics very similar to that of the data in Fig. 9) calculated by Kaptari for both PWIA and for PWIA plus FSI. (right) The ratio of $^3\text{He}(e, e'p)$ to $^3\text{H}(e, e'p)$ for the PWIA and PWIA+FSI calculations. Note that, even at this kinematic point where FSI change the cross section by a factor of almost four, the effect of the FSI on the $^3\text{He}/^3\text{H}$ ratio is much smaller [33].

Calculations by Sargsian at our proposed kinematic settings of $Q^2 = 2$ $(\text{GeV/c})^2$ and

$\theta_{rq} = 30°$ show that the effects of FSI almost entirely cancel in the ratio of ^{3}He$(e, e'p)$ to ^{3}H$(e, e'p)$ cross sections (see Fig. 14).

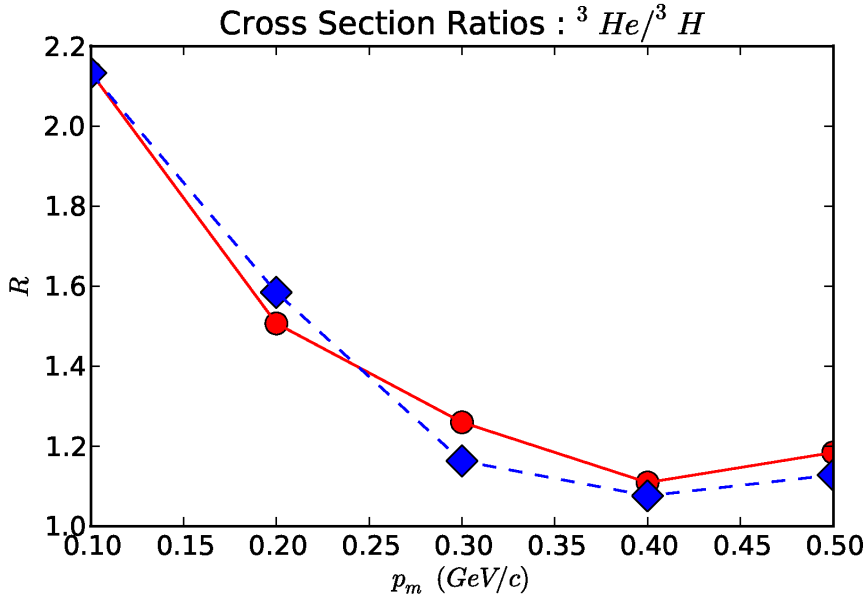FIG. 14: The ratio of the ^{3}He$(e, e'p)$ to ^{3}H$(e, e'p)$ cross sections integrated over missing energy at $Q^2 = 2$ (GeV/c)^2 and $\theta_{rq} = 30°$ for PWIA calculations (red solid curve) and FSI calculations (blue dashed curve) by Sargsian [11].

The effects of FSI only partially cancel in the ratios of ^{3}He$(e, e'p)/d(e, e'p)$ and ^{3}H$(e, e'p)/d(e, e'p)$ (see Fig. 15). We will use the measured ^{3}He$(e, e'p)/d(e, e'p)$ and ^{3}H$(e, e'p)/d(e, e'p)$ cross section ratios to test our theoretical understanding of final state interactions in these simplest of nuclei.

II.   THE MEASUREMENT

We propose to measure the ^{3}He$(e, e'p)$, ^{3}H$(e, e'p)$, and $d(e, e'p)$ cross sections for $0 \le p_m \le 500$ MeV/c in order to extract information about the ground state momentum distributions. In order to minimize the effects of competing reaction channels (MEC, IC, and FSI) and to maximize our sensitivity to the ground state momentum distribution, we will measure at

- high Q^2 ($Q^2 \approx 2$ (GeV/c)^2)
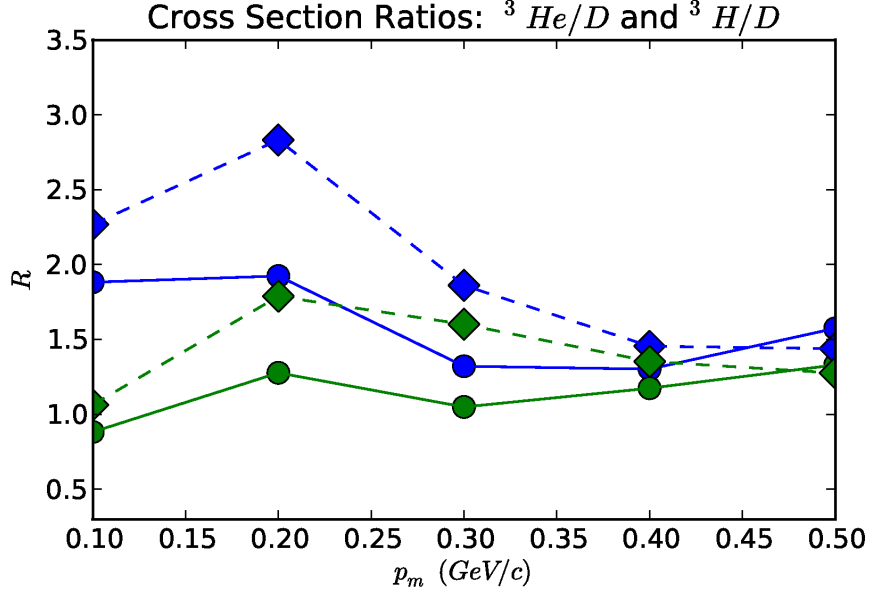
- $x = Q^2/2m\omega > 1$

FIG. 15: The ratio of the ^{3}He$(e, e'p)$ (blue) and ^{3}H$(e, e'p)$(green) to $d(e, e'p)$ cross sections integrated over missing energy at $Q^2 = 2$ (GeV/c)^2 and $\theta_{rq} = 30°$ for PWIA calculation (dashed curve) and FSI calculation (solid curve) [11].

- small θ_{rq} ($\theta_{rq} < 40°$)

In addition, we will measure the different nuclei at identical kinematic settings with the identical experimental setup. This will make it possible to probe the genuine momentum distributions with significantly smaller experimental and theoretical corrections and hence uncertainties.

Since, at fixed Q^2, cross sections increase with beam energy, we will measure the cross section with two-pass beam, $E_0 = 4.4$ GeV. This is the highest beam energy we can use and still detect the scattered electron in the Hall A HRS.

As Q^2 increases, the cross section decreases and the effects of IC and MEC decrease. In addition, the accuracy of the Eikonal approximation for calculating the effects of FSI increases. We will measure at $Q^2 = 2$ (GeV/c)^2 as a compromise between decreasing cross section and increasing ease of interpretation.

Based on deuteron results [32] and ^{3}He calculations [11, 21], we plan to reduce the effects of FSI on the cross sections by measuring the $(e, e'p)$ reaction at an angle of approximately $\theta_{rq} \approx 30°$ between the nuclear recoil and the momentum transfer.

We selected the central angle and momentum of the detected electron and knocked-out proton to be those of the deuteron. For $A = 3$ targets, this centers the kinematics close to the SRC missing energy peak where the cross section is maximum (see Fig. 9). It also ensures that we will measure both the two-body-break-up and three-body-break-up channels of $^3\text{He}(e, e'p)$.

The minimum in the $^3\text{He}(e, e'p)$ to $^3\text{H}(e, e'p)$ cross section ratio (i.e., where NN-SRC dominate) should be at about 0.4 GeV/c (see Fig. 6), at about the same point as the minimum in the ratios to the deuteron (see Fig. 4). We will measure the $^3\text{He}/^3\text{H}$ ratio out to $p_m \approx 0.5$ GeV/c and to save time we will measure the $^3\text{H}/d$ ratio out to $p_m \approx 0.4$ GeV/c. Table I shows the kinematic settings to cover this range of missing momentum.

We are requesting one day of commissioning and calibration time to measure spectrometer optics, pointing and $^1\text{H}(e, e'p)$. We expect that the systematic uncertainties due to errors in beam energy, beam charge measurements, detector efficiencies and target thickness will be very similar to the 4.5% reported in [32] for $d(e, e'p)$.

$< p_m >$ (MeV/c)	x	E_e (GeV)	θ_e	p_p (GeV/c)	θ_p	beam time $d/^3\text{H}/^3\text{He}$ (days)	total beam time (days)
	Calibrations						1
100	1.15	3.47	20.86°	1.607	48.67°	0.3/0.3/0.3	1
300	1.41	3.64	20.35°	1.352	58.55°	5/3/3	11
450	1.52	3.70	20.20°	1.229	64.93°	0/10/10	20
	Total beam time request						32

TABLE I: The central kinematics and beam time for each setting. The beam energy is 4.4 GeV and $Q^2 = 2.0$ (GeV/c)^2 for all settings.

A. MCEEP Simulations

We calculated cross sections and rates using the deuteron PWIA cross section integrated over the experimental acceptances using MCEEP, including radiative corrections. We used the parameters of the MARATHON target, with a 25-cm long target cell, a deuterium target density of 75 mg/cm^2, and a maximum beam current of 25 μA. The ^3He and ^3H targets will have approximately the same mass density as the deuterium target and will therefore have

about 2/3 of the number density. We expect the $^3\mathrm{He}(e, e'p)$ and $^3\mathrm{H}(e, e'p)$ cross sections to be about twice as large as the $d(e, e'p)$ cross section at large missing energies, compensating for the decreased number density of the $^3\mathrm{He}$ and $^3\mathrm{H}$ targets and for other expected experimental inefficiencies.

The yields as a function of missing momentum are shown in Fig. 16 for the three kinematic points. Figs. 17 and 18 show the distribution of events.
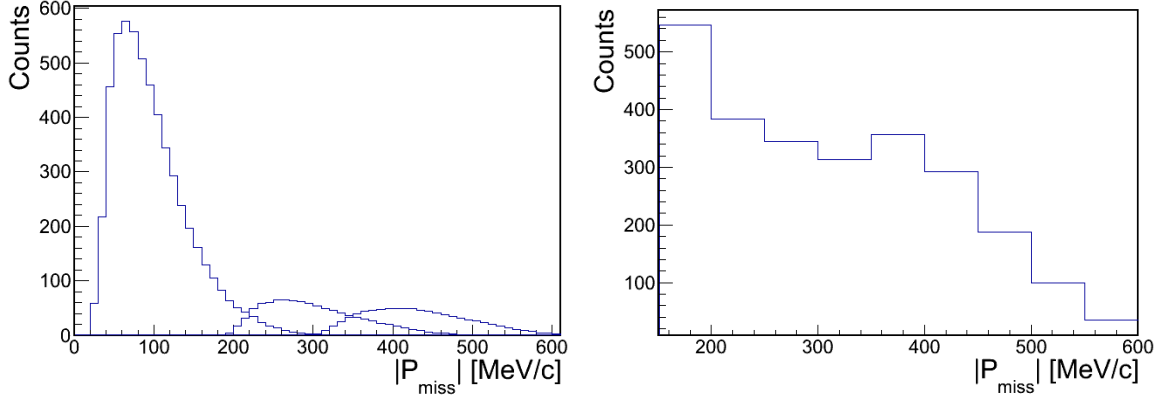

FIG. 16: (left) The expected number of events as a function of missing momentum for the three kinematic points of Table I; (right) the number of events for all three kinematic points combined, starting at $p_m = 150$ MeV/c.
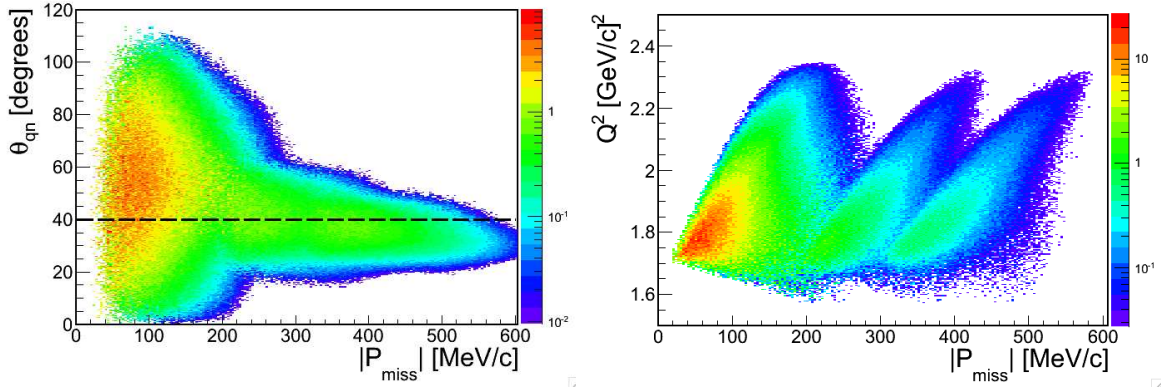

FIG. 17: (left) θ_{rq}, the angle between the recoiling system (missing momentum) and $\vec{q}$, versus the missing momentum. The dashed line shows the cut at $\theta_{rq} \leq 40°$. (right) Q^2, the square of the momentum transfer plotted versus the missing momentum. The vertical scales are logarithmic.
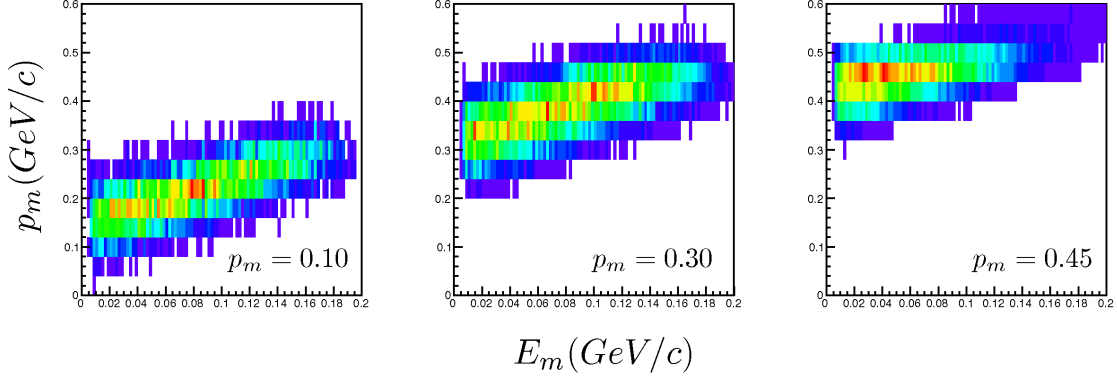
FIG. 18: The missing energy – missing momentum distribution for the three different kinematic settings. This shows the kinematic coverage and does not include cross section weighting.

B.   Expected Results

We will measure the ${}^3\mathrm{He}(e,e'p)$, ${}^3\mathrm{H}(e,e'p)$, and $d(e,e'p)$ cross sections at each value of missing momentum by integrating the cross sections over missing energy. We will then construct the cross section ratios ${}^3\mathrm{He}(e,e'p)/{}^3\mathrm{H}(e,e'p)$, ${}^3\mathrm{He}(e,e'p)/d(e,e'p)$, and ${}^3\mathrm{H}(e,e'p)/d(e,e'p)$. The expected statistical uncertainties are shown in Figs. 19, 20 and 21.
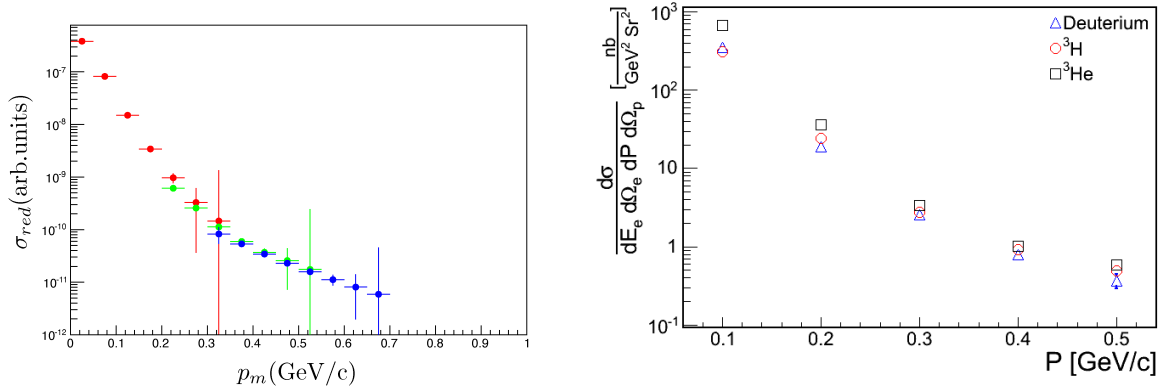

FIG. 19: (left) The expected statistical uncertainties in the proposed measured reduced cross section integrated over missing energy as a function of missing momentum for each kinematic setting (all three nuclei will have approximately the same uncertainties). (right) The expected statistical uncertainties in the proposed measured cross sections for ${}^3\mathrm{He}(e,e'p)$, ${}^3\mathrm{H}(e,e'p)$, and $d(e,e'p)$ integrated over missing energy as a function of missing momentum.
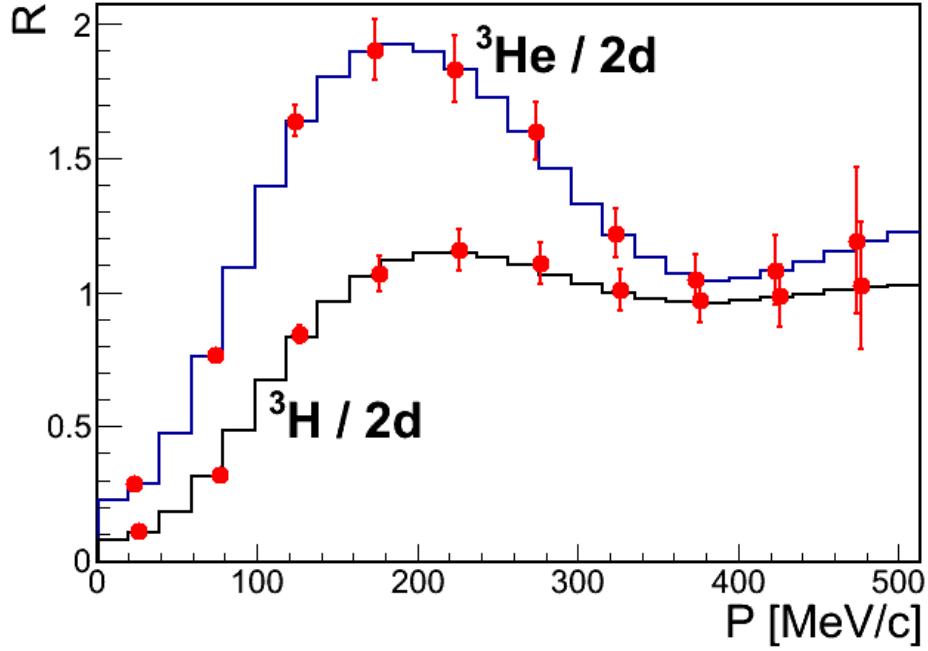
FIG. 20: The expected statistical uncertainties in the proposed measured cross section ratios of $^3\mathrm{He}(e,e'p)/2d(e,e'p)$ and $^3\mathrm{H}(e,e'p)/2d(e,e'p)$ as a function of missing momentum. (The factor of two in the ratio is the expected cross section ratio at large missing momenta as measured in inclusive $A(e,e')$ scattering ratios [13].)
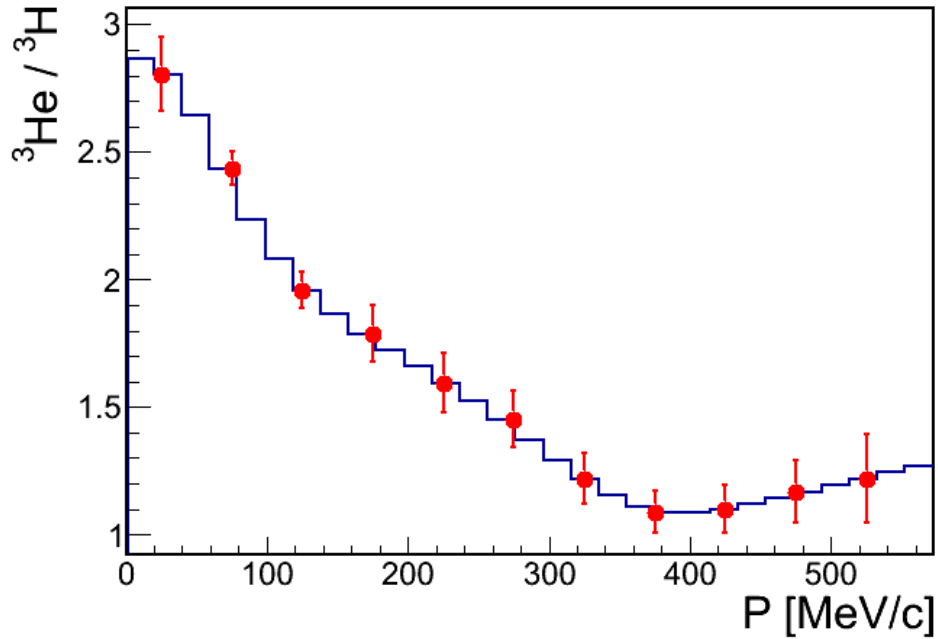

FIG. 21: The expected statistical uncertainties in the proposed measured cross section ratios of $^3\mathrm{He}(e,e'p)/^3\mathrm{H}(e,e'p)$ as a function of missing momentum.

III. SUMMARY

Fully understanding few-nucleon systems is vital to our understanding of nuclear physics. We propose to take advantage of a unique opportunity to measure the cross sections of $^3\text{H}(e, e'p)$, $^3\text{He}(e, e'p)$, and $d(e, e'p)$ in Hall A in order to determine the momentum distributions of asymmetric nuclei. $^3\text{H}(e, e'p)$ has never been measured before and $^3\text{He}(e, e'p)$ has never been measured in kinematics which minimize the effects of final state interactions (FSI), meson exchange currents, and isobar configurations.

By forming the cross section ratio of $^3\text{He}(e, e'p)$ to $^3\text{H}(e, e'p)$, the remaining effects of FSI almost entirely cancel, allowing us to extract the ratio of their momentum distributions with unprecedented precision. We propose to measure this ratio from $p_m = 0$ where independent nucleons dominate (and the ratio should be about two) to $p_m = 0.5$ GeV/c where nucleons belonging to short range correlations (SRC) dominate (and the ratio should be about one).

We also propose to measure the absolute cross sections of these reactions in order to provide a stringent test of theoretical models. These models will face different challenges in calculating the absolute cross sections, the cross section ratios $^3\text{He}(e, e'p)/d(e, e'p)$ and $^3\text{H}(e, e'p)/d(e, e'p)$, and the cross section ratio $^3\text{He}(e, e'p)/^3\text{H}(e, e'p)$.

We propose to measure these cross sections using the Hall A HRS spectrometers and the MARATHON target. Radioactive targets in general and tritium targets in particular pose serious safety issues and are thus very difficult to install. The MARATHON target will only be at Jefferson Lab for a brief period. This will be the only opportunity to measure $^3\text{H}(e, e'p)$. It is crucial to take advantage of this opportunity to fill a gaping hole in our knowledge of few-nucleon systems.

We request 32 days of beam time to measure $^3\text{H}(e, e'p)$, $^3\text{He}(e, e'p)$, and $d(e, e'p)$.

[1] R. Subedi et al., Science **320**, 1476 (2008).

[2] R. Shneor et al., Phys. Rev. Lett. **99**, 072501 (2007).

[3] E. Piasetzky, M. Sargsian, L. Frankfurt, M. Strikman, and J. W. Watson, Phys. Rev. Lett. **97**, 162504 (2006).

[4] R. Schiavilla, R. B. Wiringa, S. C. Pieper, and J. Carlson, Physical Review Letters **98**, 132501 (2007).

[5] M. M. Sargsian, T. V. Abrahamyan, M. I. Strikman, and L. L. Frankfurt, Phys. Rev. **C71**, 044615 (2005), nucl-th/0501018.

[6] M. Alvioli, C. C. degli Atti, and H. Morita, Phys. Rev. Lett. **100**, 162503 (2008).

[7] M. M. Sargsian (2012), 1210.3280.

[8] L. B. Weinstein, E. Piasetzky, D. W. Higinbotham, J. Gomez, O. Hen, and R. Shneor, Phys. Rev. Lett. **106**, 052301 (2011).

[9] O. Hen, E. Piasetzky, and L. B. Weinstein, Phys. Rev. C **85**, 047301 (2012).

[10] O. Benhar and I. Sick (2012), 1207.4595.

[11] M. Sargsian, *Private communication.*

[12] L. Frankfurt, M. Sargsian, and M. Strikman, International Journal of Modern Physics A **23**, 2991 (2008), http://www.worldscientific.com/doi/pdf/10.1142/S0217751X08041207, URL `http://www.worldscientific.com/doi/abs/10.1142/S0217751X08041%207`.

[13] N. Fomin et al., Phys. Rev. Lett. **108**, 092502 (2012).

[14] H. Baghdasaryan et al. (CLAS Collaboration), Phys. Rev. Lett. **105**, 222501 (2010).

[15] K. Egiyan et al. (CLAS Collaboration), Phys. Rev. Lett. **96**, 082501 (2006).

[16] R. Wiringa, *Private communication.*

[17] R. B. Wiringa, V. G. J. Stoks, and R. Schiavilla, Phys. Rev. C **51**, 38 (1995).

[18] S. Veerasamy and W. N. Polyzou, Phys. Rev. C **84**, 034003 (2011).

[19] S. C. Pieper and R. B. Wiringa, Annual Review of Nuclear and Particle Science **51**, 53 (2001).

[20] M. Alvioli, C. Ciofi degli Atti, L. P. Kaptari, C. B. Mezzetti, and H. Morita, Phys. Rev. C **87**, 034603 (2013), URL `http://link.aps.org/doi/10.1103/PhysRevC.87.034603`.

[21] C. Ciofi degli Atti, *Private communication.*

[22] A. Bussiere et al., Nucl. Phys. **A365**, 349 (1981).

[23] K. Blomqvist et al., Phys. Lett. **B429**, 33 (1998).

[24] W. U. Boeglin, H. Arenhövel, K. I. Blomqvist, R. Böhm, M. Distler, R. Edelhoff, I. Ewald, R. Florizone, J. Friedrich, R. Geiges, et al., Phys. Rev. C **78**, 054001 (2008).

[25] P. E. Ulmer, K. A. Aniol, H. Arenhövel, J.-P. Chen, E. Chudakov, D. Crovelli, J. M. Finn, K. G. Fissum, O. Gayou, J. Gomez, et al., Phys. Rev. Lett. **89**, 062301 (2002).

[26] M. M. Rvachev et al. (Jefferson Lab Hall A Collaboration), Phys. Rev. Lett. **94**, 192302 (2005).

[27] F. Benmokhtar et al. (Jefferson Lab Hall A Collaboration), Phys. Rev. Lett. **94**, 082305 (2005).

[28] C. Ciofi degli Atti and L. P. Kaptari, Phys. Rev. Lett. **95**, 052502 (2005), URL `http://link.aps.org/doi/10.1103/PhysRevLett.95.052502`.

[29] J.-M. Laget, *Photo and electrodisintegration of few body systems revisited* (2003).

[30] J.-M. Laget, Phys. Lett. **B609**, 49 (2005).

[31] M. Alvioli, C. C. d. Atti, and L. P. Kaptari, Phys. Rev. C **81**, 021001 (2010), URL `http://link.aps.org/doi/10.1103/PhysRevC.81.021001`.

[32] W. U. Boeglin, L. Coman, P. Ambrozewicz, K. Aniol, J. Arrington, G. Batigne, P. Bosted, A. Camsonne, G. Chang, J. P. Chen, et al. (For the Hall A Collaboration), Phys. Rev. Lett. **107**, 262501 (2011).

[33] L. Kaptari, *Private communication.*